BOUNDED SPARSE PHOTON-LIMITED IMAGE RECOVERY

Lasith Adhikari and Roummel F. Marcia

Department of Applied Mathematics, University of California, Merced, Merced, CA 95343 USA

ABSTRACT

In photon-limited image reconstruction, the behavior of noise at the detector end is more accurately modeled as a Poisson point process than the common choice of a Gaussian distribution. As such, to recover the original signal more accurately, a penalized negative Poisson log-likelihood function – and not a least-squares function – is minimized. In many applications, including medical imaging, additional information on the signal of interest is often available. Specifically, its maximum and minimum amplitudes might be known *a priori*. This paper describes an approach that incorporates this information into a sparse photon-limited recovery method by the inclusion of upper and lower bound constraints. We demonstrate the effectiveness of the proposed approach on two different low-light deblurring examples.

Index Terms— Photon-limited imaging, Poisson noise, bounded sparse approximation, convex optimization, wavelets.

1. INTRODUCTION

Signal recovery under low-light conditions arises in many applications, including medical imaging [1, 2], astronomy [3, 4], and security and defense [5, 6]. In low photon context, the arrival of photons at the detector is typically modeled by the inhomogeneous Poisson process:

$$y \sim \text{Poisson}(Af^*),$$

where $y \in \mathbb{Z}_+^m$ is the vector of observed photon counts, $A \in \mathbb{R}_+^{m\times n}$ is the linear projection matrix, and $f^* \in \mathbb{R}_+^n$ is the nonnegative true signal of interest (see e.g., [7, 8]). If the signal to be reconstructed is known to be sparse, then it can be approximated by solving a Poisson inverse problem with a sparsity-promoting penalty (see e.g., [9, 10, 11, 12]).

In addition to sparsity and nonnegativity, other intensity information about the true signal may be known. In particular, its maximum and minimum amplitudes at specific regions might be known *a priori*. In medical imaging, structural information such as tissue geometries are used to improve the accuracy of tomography. For example, in near infrared diffuse optical tomography, structural priors from magnetic resonance imaging are incorporated to limit smoothing across their shared boundaries and adjust the image smoothness [13, 14, 15]. These structural priors can be expressed as bounds on the signal intensity, and as such, they can be incorporated into the photon-limited image recovery problem to enhance the quality of the reconstruction. This paper describes an optimization method (based on the SPIRAL approach [12]) that includes upper and lower bound constraints that model additional signal intensity information. We demonstrate the effectiveness of the proposed approach on two different low-light deblurring examples.

This work was supported by National Science Foundation Grant CMMI-1333326. Lasith Adhikari's research is supported by the UC Merced Graduate Student Opportunity Fellowship Program.

2. PROBLEM FORMULATION

When the maximum and minimum signal intensity information is known, the sparsity-promoting Poisson intensity reconstruction problem has the following constrained minimization form:

$$\begin{aligned}\hat{f} \;=\; &\underset{f\in\mathbb{R}^n}{\arg\min} \quad \Phi(f) \equiv F(f) + \tau\|f\|_1 \\ &\text{subject to} \;\; b_L \le f \le b_U,\end{aligned}$$

where $\tau > 0$ is the regularization parameter and $F(f)$ is the negative Poisson log-likelihood function

$$F(f) = \mathbb{1}^T Af - \sum_{i=1}^{m} y_i \log(e_i^T Af + \beta),$$

where $\mathbb{1}$ is an m-vector of ones, e_i is the ith canonical basis unit vector, $\beta > 0$ (typically $\beta \ll 1$ to avoid the singularity at $f = 0$) (see e.g., [16]). Our proposed approach builds upon the the SPIRAL framework in [12], which defines a sequence of quadratic subproblems, where $F(f)$ is approximated by a second-order Taylor series expansion, where the Hessian matrix is replaced by a scaled identity matrix $\alpha_k I$, where $\alpha_k > 0$ (see e.g., [17, 18]). In our proposed approach, these quadratic subproblems are of the form

$$\begin{aligned}f^{k+1} \;=\; &\underset{f\in\mathbb{R}^n}{\arg\min} \quad \tfrac{1}{2} \parallel f - s^k \parallel_2^2 \; + \tfrac{\tau}{\alpha_k}\|f\|_1 \\ &\text{subject to} \quad b_L \le f \le b_U,\end{aligned}$$

where $s^k = f^k - \frac{1}{\alpha_k}\nabla F(f^k)$. If the signal of interest is sparse in some orthonormal basis W, then the penalty term $\|f\|_1$ is

replaced by $\|\theta\|_1$, where $\theta = W^T f$. Then the minimization subproblem becomes

$$\theta^{k+1} = \underset{\theta\in\mathbb{R}^n}{\arg\min} \quad \phi^k(\theta) = \tfrac{1}{2}\|\theta - s^k\|_2^2 + \tfrac{\tau}{\alpha_k}\|\theta\|_1, \quad \text{subject to } b_L \le W\theta \le b_U. \tag{1}$$

We note that typically, $b_L = 0$, but we do not make that assumption here. We can solve this minimization problem by solving its Lagrangian dual. The discussion below follows [12] very closely. Our main contribution is the extension of the constraints to general bounds and the inclusion of a convergence proof for the subproblem minimization.

First, we introduce $u, v \in \mathbb{R}^n$ with $u, v \ge 0$ and write $\theta = u - v$ so that $\phi^k(\theta)$ in (1) is differentiable [10, 12]:

$$(u^{k+1}, v^{k+1}) = \underset{u,v\in\mathbb{R}^n}{\arg\min} \quad \tfrac{1}{2}\|u - v - s^k\|_2^2 + \tfrac{\tau}{\alpha_k}\mathbb{1}^T(u+v) \quad \text{subject to } u, v \ge 0, b_L \le W(u-v) \le b_U. \tag{2}$$

Note, however, that the new problem now has twice as many parameters and has additional nonnegativity constraints on the new parameters. The last constraints can be expressed as $W(u-v) - b_L \ge 0$ and $b_U - W(u-v) \ge 0$. The Lagrangian function corresponding to (2) is given by

$$\begin{aligned}\mathscr{L}(u, v, \lambda_1, \lambda_2, \lambda_3, \lambda_4) &= \tfrac{1}{2}\|u - v - s^k\|_2^2 \\ &+ \tfrac{\tau}{\alpha_k}\mathbb{1}^T(u+v) - \lambda_1^T u - \lambda_2^T v \\ &- \lambda_3^T(W(u-v) - b_L) - \lambda_4^T(b_U - W(u-v)),\end{aligned}$$

where $\lambda_1, \lambda_2, \lambda_3, \lambda_4 \in \mathbb{R}^n$ are the Lagrange multipliers corresponding to the constraints in (2). Differentiating $\mathscr{L}$ with respect to u and v and setting the derivatives to zero yields

$$\begin{aligned} u - v &= s^k + \lambda_1 - \tfrac{\tau}{\alpha_k}\mathbb{1} + W^T\lambda_3 - W^T\lambda_4, \text{ and} \\ \lambda_2 &= \tfrac{2\tau}{\alpha_k}\mathbb{1} - \lambda_1. \end{aligned} \tag{3}$$

Then it follows that $\frac{\tau}{\alpha_k}\mathbb{1}^T(u+v) - \lambda_1^T u - \lambda_2^T v = \frac{\tau}{\alpha_k}\mathbb{1}^T(u-v) - \lambda_1^T(u-v)$ in $\mathscr{L}$. Therefore

$$\begin{aligned}\mathscr{L}(u, v, \lambda_1, \lambda_2, \lambda_3, \lambda_4) = \ & \tfrac{1}{2}\|u - v\|_2^2 + \tfrac{1}{2}\|s^k\|_2^2 \\ &- (u-v)^T(s^k + \lambda_1 - \tfrac{\tau}{\alpha_k}\mathbb{1} + W^T\lambda_3 - W^T\lambda_4) \\ &+ \lambda_3^T b_L - \lambda_4^T b_U.\end{aligned}$$

Substituting $u - v$ from (3) in $\mathscr{L}$, we obtain the Lagrangian dual function independent of the primal variables, u and v:

$$\begin{aligned} g(\lambda_1, \lambda_3, \lambda_4) = & -\tfrac{1}{2}\|s^k + \lambda_1 - \tfrac{\tau}{\alpha_k}\mathbb{1} + W^T(\lambda_3 - \lambda_4)\|_2^2 \\ &+ \lambda_3^T b_L - \lambda_4^T b_U + \frac{1}{2}\|s^k\|_2^2. \end{aligned}$$

Next, let $\gamma = \lambda_1 - \frac{\tau}{\alpha_k}\mathbb{1}$. For the Lagrange dual problem corresponding to (2), the Lagrange multipliers $\lambda_i \ge 0$ for $i \in \{1, 2, 3, 4\}$. Since $0 \le \lambda_2 = \frac{2\tau}{\alpha_k}\mathbb{1} - \lambda_1 = \frac{\tau}{\alpha_k}\mathbb{1} - \gamma$ and $0 \le \lambda_1 = \gamma + \frac{\tau}{\alpha_k}\mathbb{1}$, then γ satisfies $-\frac{\tau}{\alpha_k}\mathbb{1} \le \gamma \le \frac{\tau}{\alpha_k}\mathbb{1}$. The Lagrange dual problem associated with (2) is thus given by

$$\begin{aligned}\underset{\gamma,\lambda_3,\lambda_4\in\mathbb{R}^n}{\text{minimize}} \ & h(\gamma, \lambda_3, \lambda_4) = \tfrac{1}{2}\|s^k + \gamma + W^T(\lambda_3 - \lambda_4)\|_2^2 \\ &- \lambda_3^T b_L + \lambda_4^T b_U - \tfrac{1}{2}\|s^k\|_2^2 \\ \text{subject to } & \lambda_3, \lambda_4 \ge 0, \ -\tfrac{\tau}{\alpha_k}\mathbb{1} \le \gamma \le \tfrac{\tau}{\alpha_k}\mathbb{1}. \end{aligned} \tag{4}$$

At the dual optimal values $\gamma^\star$, $\lambda_3^\star$, and $\lambda_4^\star$, the primal iterate θ^{k+1} is given by $\theta^{k+1} = u^{k+1} - v^{k+1} = s^k + \gamma^\star + W^T(\lambda_3^\star - \lambda_4^\star)$. We note that the duality gap for (2) and its dual (4) is zero, i.e., $\phi^k(\theta^{k+1}) = -h(\gamma^\star, \lambda_3^\star, \lambda_4^\star)$ because (2) satisfies (a weakened) Slater's condition [19]. In addition, the function $-h(\gamma, \lambda_3, \lambda_4)$ is a lower bound on $\phi^k(\theta)$ at any dual feasible point.

We note that the objective function $h(\gamma, \lambda_3, \lambda_4)$ can be written as

$$\begin{aligned} h(\gamma, \lambda_3, \lambda_4) = & \{\tfrac{1}{2}\|\gamma\|_2^2 + \gamma^T s^k\} + \gamma^T W^T(\lambda_3 - \lambda_4) \\ &+ \{\tfrac{1}{2}\|\lambda_3 - \lambda_4\|_2^2 + (\lambda_3 - \lambda_4)^T W s^k - \lambda_3^T b_L + \lambda_4^T b_U\}. \end{aligned}$$

We minimize the objective function $h(\gamma, \lambda_3, \lambda_4)$ by solving for γ, λ_3, and λ_4 alternatingly, which is done by taking the partial derivatives of $h(\gamma, \lambda_3, \lambda_4)$ and setting them to zero. Each component is then constrained to satisfy the bounds in (4). We now describe each step more explicitly.

Step 1. Given $\lambda_3^{(j-1)}$ and $\lambda_4^{(j-1)}$ from the previous iterate, solve

$$\gamma^{(j)} = \underset{\gamma\in\mathbb{R}^n}{\arg\min} \quad \tfrac{1}{2}\|\gamma\|_2^2 + \gamma^T s^k + \gamma^T W^T(\lambda_3^{(j-1)} - \lambda_4^{(j-1)}) \quad \text{subject to } -\tfrac{\tau}{\alpha_k}\mathbb{1} \le \gamma \le \tfrac{\tau}{\alpha_k}\mathbb{1}. \tag{5}$$

The solution to (5) is obtained via thresholding:

$$\gamma^{(j)} = \text{mid}\Big\{-\tfrac{\tau}{\alpha_k}\mathbb{1}, -s^k - W^T\Big(\lambda_3^{(j-1)} - \lambda_4^{(j-1)}\Big), \tfrac{\tau}{\alpha_k}\mathbb{1}\Big\}, \tag{6}$$

where the operator $\text{mid}\{a, b, c\}$ chooses the middle value of the three arguments component-wise.

Step 2. Given $\gamma^{(j)}$, solve

$$\begin{aligned}(\lambda_3^{(j)}, \lambda_4^{(j)}) = \underset{\lambda_3,\lambda_4\in\mathbb{R}^n}{\arg\min} \ & \mathcal{L}(\lambda_3, \lambda_4) \equiv \tfrac{1}{2}\|\lambda_3 - \lambda_4\|_2^2 \\ &+ \lambda_3^T\big(W(s^k + \gamma^{(j)}) - b_L\big) \\ &+ \lambda_4^T\big(b_U - W(s^k + \gamma^{(j)})\big) \\ \text{subject to } & \lambda_3, \lambda_4 \ge 0. \end{aligned} \tag{7}$$

The minimization problem (7) has the following solution. Noting $\frac{1}{2}\|\lambda_3 - \lambda_4\|_2^2 = \frac{1}{2}\|\lambda_3\|_2^2 - \lambda_3^T\lambda_4 + \frac{1}{2}\|\lambda_4\|_2^2$, and letting $r_L^{(j)} = W(s^k + \gamma^{(j)}) - b_L$ and $r_U^{(j)} = b_U - W(s^k + \gamma^{(j)})$,

then (7) can be written as

$$(\lambda_3^{(j)}, \lambda_4^{(j)}) = \underset{\lambda_3,\lambda_4\in\mathbb{R}^n}{\arg\min} \quad \tfrac{1}{2}\|\lambda_3\|_2^2 + \lambda_3^T r_L^{(j)} - \lambda_3^T\lambda_4 + \tfrac{1}{2}\|\lambda_4\|_2^2 + \lambda_4^T r_U^{(j)} \quad \text{subject to } \lambda_3, \lambda_4 \geq 0. \tag{8}$$

Note that if $r_L^{(j)} \geq 0$ and $r_U^{(j)} \geq 0$, i.e., $b_L \leq W(s^k + \gamma^{(j)}) \leq b_U$, then $\mathcal{L}(\lambda_3, \lambda_4) \geq 0$ for $\lambda_3, \lambda_4 \geq 0$, and is therefore minimized at $\lambda_3 = \lambda_4 = 0$. We now assume otherwise. Computing the gradient of $\mathcal{L}(\lambda_3, \lambda_4)$ with respect to λ_3 and λ_4 yields $\nabla_{\lambda_3}\mathcal{L}(\lambda_3, \lambda_4) = \lambda_3 + r_L^{(j)} - \lambda_4$ and $\nabla_{\lambda_4}\mathcal{L}(\lambda_3, \lambda_4) = \lambda_4 + r_U^{(j)} - \lambda_3$. For each i, unless $(b_L)_i = (b_U)_i$, both $(\nabla_{\lambda_3}\mathcal{L})_i$ and $(\nabla_{\lambda_4}\mathcal{L})_i$ cannot be simultaneously 0 (since this implies $(r_L^{(j)})_i + (r_U^{(j)})_i = 0$, or equivalently, $(b_U)_i - (b_L)_i = 0$). Therefore, the components of the gradient of the minimizer must be 0 or the corresponding components of the minimizer must lie on the boundary, i.e., $(\nabla_{\lambda_3}\mathcal{L})_i = 0$ and $(\lambda_4)_i = 0$, or $(\lambda_3)_i = 0$ and $(\nabla_{\lambda_4}\mathcal{L})_i = 0$. These conditions define the values of the solutions $\lambda_3^{(j)}$ and $\lambda_4^{(j)}$:

$$\begin{aligned} \lambda_3^{(j)} &= [-r_L^{(j)}]_+ = [-W(s^k + \gamma^{(j)}) + b_L]_+ \\ \lambda_4^{(j)} &= [-r_U^{(j)}]_+ = [\ W(s^k + \gamma^{(j)}) - b_U]_+. \end{aligned}$$

where the operator $[\,\cdot\,]_+ = \max\{\,\cdot\,, 0\}$ component-wise.

Convergence. We prove the convergence of this alternating minimization strategy from techniques found in [20]. Let

$$\begin{aligned} f(\gamma, \lambda_3, \lambda_4) &= \gamma^T W^T(\lambda_3 - \lambda_4) \\ g_1(\gamma) &= \tfrac{1}{2}\|\gamma\|_2^2 + \gamma^T s^k \\ g_2(\lambda_3, \lambda_4) &= \tfrac{1}{2}\|\lambda_3 - \lambda_4\|_2^2 + (\lambda_3 - \lambda_4)^T W s^k \\ &\quad -\lambda_3^T b_L + \lambda_4^T b_U \end{aligned}$$

so that $h(\gamma, \lambda_3, \lambda_4) = f(\gamma, \lambda_3, \lambda_4) + g_1(\gamma) + g_2(\lambda_3, \lambda_4)$. Note the following: (A) Both functions g_1 and g_2 are continuous functions whose domains are closed. Consequently, they are closed (see Sec. A.3.3 in [19]). (B) f is bilinear in γ and in (λ_3, λ_4). Therefore, it is a continuously differentiable convex function. (C) The gradient of f with respect to γ is constant, and therefore $\nabla_\gamma f$ is Lipschitz continuous. (D) The gradient of f with respect to (λ_3, λ_4) is constant, and therefore $\nabla_{\lambda_3,\lambda_4} f$ is Lipschitz continuous. (E) Since the primal problem (1) has a continuous objective function and has a closed and bounded domain, it must have a minimum by the Extreme Value Theorem. Because the duality gap is zero, i.e., $\phi^k(\theta^{k+1}) = -h(\gamma^\star, \lambda_3^\star, \lambda_4^\star)$, the dual problem (4) must have a solution. In addition, the subproblems (5) and (7) have explicit minimizers. With these, the assumptions needed to apply Lemma 3.2 in [20] are satisfied. In particular, we obtain the following convergence result:

Theorem 1: Let $\{(\gamma^{(j)}, \lambda_3^{(j)}, \lambda_4^{(j)})\}_{j\geq 0}$ be the sequence generated by the proposed alternating minimization method. Any accumulation point of $\{(\gamma^{(j)}, \lambda_3^{(j)}, \lambda_4^{(j)})\}$ is a stationary point of problem (4).

Feasibility. We now show that at the end of each iteration j, the approximate solution $\theta^{(j)} = s^k + \gamma^{(j)} + W^T(\lambda_3^{(j)} - \lambda_4^{(j)})$ to (1) is feasible with respect to the constraint $b_L \leq W\theta \leq b_U$. First, note that

$$\begin{aligned} W\theta^{(j)} &= Ws^k + W\gamma^{(j)} + \lambda_3^{(j)} - \lambda_4^{(j)} \\ &= W(s^k + \gamma^{(j)}) + \Big[b_L - W(s^k + \gamma^{(j)})\Big]_+ \\ &\quad - \Big[W(s^k + \gamma^{(j)}) - b_U\Big]_+. \end{aligned} \tag{9}$$

We note that (9) is equivalent to

$$W\theta^{(j)} = \text{mid}\{b_L, W(s^k + \gamma^{(j)}), b_U\}.$$

Thus, we can terminate the iterations for the dual problem early and still obtain a feasible point.

3. NUMERICAL RESULTS

We investigate the effectiveness of the proposed bounded SPIRAL-ℓ_1 (B-SPIRAL-ℓ_1) method by solving two image deblurring problems. In both experiments, the blurry observations are obtained from Af^*, where the signal f^* is convolved with a 5×5 blur matrix, whose action is represented by the matrix A. The MATLAB's `poissrnd` function is used to add Poisson noise. Here, we used the Daubechies-2 (DB-2) wavelet basis for W.

We implemented the B-SPIRAL-ℓ_1 algorithm by including constraints to the existing SPIRAL approach [21] to solve subproblem (1). The algorithm is initialized using the lower and upper bound information incorporated $A^T y$ and terminates if the relative difference between consecutive iterates converged to $\|f^{k+1} - f^k\|_2/\|f^k\|_2 \leq 10^{-6}$. Similar to the SPIRAL approach, we define 30 as the minimum number of iterations to avoid any issues with premature termination. Finally, we compare the results with nonnegatively constrained SPIRAL-ℓ_1 method based on RMSE $(\%) = 100 \cdot \|\hat{f} - f^*\|_2/\|f^*\|_2$. The final SPIRAL-$\ell_1$ reconstructions are thresholded using the same bounds used in B-SPIRAL-ℓ_1. The regularization parameters (τ) for both experiments are optimized to get the minimum RMSE value.

3.1. QR code deblurring

In this experiment, we wish to recover a Quick Response (QR) code of size 512×512 (see Fig. 1(a)) from the Poisson-noise corrupted blurry image (see Fig. 1(b) and the red zoomed region in Fig. 1(c)). We set b_U as the peak intensity of f^*, i.e., b_U = 3e+4, and b_L as the zero intensity.

The SPIRAL-ℓ_1 method took 16.52 sec (32 iterations) to converge, and its reconstruction ($\hat{f}_S$) has RMSE $= 18.92\%$. In contrast, the proposed B-SPIRAL-ℓ_1 method took 25.06

(a) True image f^* (b) Observation y (c) Zoomed region

Fig. 1. Experimental setup: (a) True QR code image f^*, (b) noisy and blurry observation y with mean photon count 5.7, (c) a zoomed region of y.

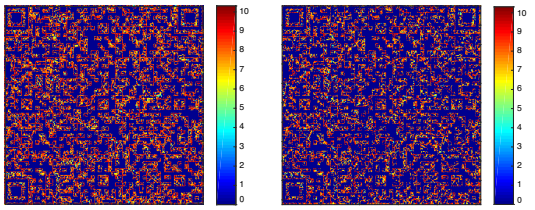

(a) $\log(1+|f^*-\hat{f}_S|)$ (RMSE = 18.92%) (b) $\log(1+|f^*-\hat{f}_B|)$ (RMSE = 16.42 %)

Fig. 2. (a) Log magnitude of error between the true image, f^*, and the SPIRAL-ℓ_1 reconstruction $\hat{f}_S$, (b) Log magnitude of error between f^* and the proposed B-SPIRAL-ℓ_1 reconstruction $\hat{f}_B$. RMSE $(\%) = 100 \cdot \|\hat{f}-f^*\|_2/\|f^*\|_2$. Note the lower RMSE for the proposed method's reconstruction, $\hat{f}_B$, whose log error is closer to zero (represented in blue) than the original method.

sec (30 iterations) to converge, but its reconstruction ($\hat{f}_B$) has RMSE $= 16.42\%$. The B-SPIRAL-ℓ_1 improvements can be best seen in the magnitude of the log error between the true signal f^* and the reconstructions (see Figs. 2(a) and (b)). Note that the $\hat{f}_B$ reconstruction more closely matches the original signal f^* than the $\hat{f}_S$ reconstruction by the prevalence of blue regions in Fig. 2(b).

3.2. Shepp-Logan phantom image deblurring

In the reconstruction of optical images, anatomical information (the tissue shape and/or structure) from x-ray computed tomography (CT) or magnetic resonance imaging (MRI) can be used to improve the spatial resolution [22, 23]. In this experiment, we wish to apply a similar approach to recover the Shepp-Logan phantom image of size 128×128 from the observed image (see Fig. 3(a) and (b) respectively), when the tissue outer boundary is known. More specifically, we incorporate that outer boundary as a structural information (see Fig. 3(c)), where the lower and upper bound intensities are known based on the region (i.e., 0 and 1e+6 are outside and inside tissue maximum intensities respectively).

For this problem, the SPIRAL-ℓ_1 method took 1.89 sec (39 iterations) to converge, and its reconstruction ($\hat{f}_S$) has RMSE $= 21.57\%$. The proposed B-SPIRAL-ℓ_1 method took 1.98 sec (30 iterations) to converge, and its reconstruction ($\hat{f}_B$) has a lower RMSE $= 18.85\%$ (see Figs. 4(a) and (b)). Note the more accurate reconstruction along the top edges as well as the overall improved accuracy within the body (represented in yellow) in comparison to the $\hat{f}_S$ reconstruction.

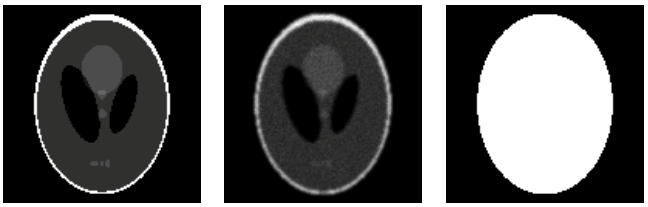

(a) True image f^* (b) Observation y (c) Mask

Fig. 3. Experimental setup: (a) True phantom image f^*, (b) noisy and blurry observation y with mean photon count 45.8, (c) mask with prior structural information.

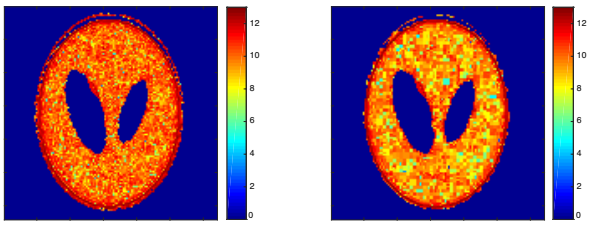

(a) $\log(1+|f^*-\hat{f}_S|)$ (RMSE = 21.57%) (b) $\log(1+|f^*-\hat{f}_B|)$ (RMSE = 18.85%)

Fig. 4. (a) Log magnitude of error between the true image, f^*, and $\hat{f}_S$, and (b) Log magnitude of error between f^* and $\hat{f}_B$. RMSE $(\%) = 100 \cdot \|\hat{f}-f^*\|_2/\|f^*\|_2$. Note the proposed method's log error is lower on the whole (represented in yellow) in contrast to the mostly orange in (a).

4. CONCLUSION

In this paper, we formulated a sparsity-promoting bound-constrained photon-limited image recovery method by solving the dual problem based on an alternating minimization strategy. The utilization of any available prior image information has proven very successful for accurately recovering images. We demonstrate that the proposed B-SPIRAL-ℓ_1 method leads to more accurate reconstructions than the simply thresholded solutions from the nonnegatively constrained minimization method.

Acknowledgments. We thank Prof. Rebecca Willett for fruitful discussions related to this work.

5. REFERENCES

[1] J. A. Sorenson and M. E. Phelps, *Physics in Nuclear Medicine*, Grune & Stratton, 1980.

[2] J. A. Fessler and H. Erdoğan, "A paraboloidal surrogates algorithm for convergent penalized-likelihood emission image reconstruction," in *Proc. IEEE Nuc. Sci. Symp. Med. Im. Conf.*, 1998.

[3] R. L. Lucke and L. J. Rickard, "Photon-limited synthetic-aperture imaging for planet surface studies," *Appl. Opt.*, vol. 41, no. 24, pp. 5084–5095, Aug 2002.

[4] J. Starck and F. Murtagh, *Astronomical Image and Data Analysis*, Springer, 2002.

[5] L. Hai-Bo, H. Zhong, N. Karpowicz, Y. Chen, and Z. Xi-Cheng, "Terahertz spectroscopy and imaging for defense and security applications," *Proceedings of the IEEE*, vol. 95, no. 8, pp. 1514–1527, Aug 2007.

[6] M. Cho and B. Javidi, "Three-dimensional photon counting double-random-phase encryption," *Optics Letters*, vol. 38, no. 17, pp. 3198–3201, Sep 2013.

[7] D. L. Snyder and M. I. Miller, *Random Point Processes in Time and Space*, Springer, 1991.

[8] R. D. Nowak and E. D. Kolaczyk, "A statistical multiscale framework for poisson inverse problems," *IEEE Transactions on Information Theory*, vol. 46, no. 5, pp. 1811–1825, Aug 2000.

[9] F.-X. Dupé, J. M. Fadili, and J.-L. Starck, "A proximal iteration for deconvolving Poisson noisy images using sparse representations," *IEEE Transactions on Image Processing*, vol. 18, no. 2, pp. 310–321, Feb 2009.

[10] M. A. T. Figueiredo and J. M. Bioucas-Dias, "Restoration of poissonian images using alternating direction optimization," *IEEE Transactions on Image Processing*, vol. 19, no. 12, pp. 3133–3145, 2010.

[11] N. Pustelnik, C. Chaux, and J. Pesquet, "Parallel proximal algorithm for image restoration using hybrid regularization," *IEEE Transactions on Image Processing*, vol. 20, no. 9, pp. 2450–2462, Sept 2011.

[12] Z. T. Harmany, R. F. Marcia, and R. M. Willett, "This is SPIRAL-TAP: Sparse Poisson intensity reconstruction algorithms; theory and practice," *IEEE Trans. on Image Processing*, vol. 21, no. 3, pp. 1084–1096, March 2012.

[13] P. K. Yalavarthy, B. W. Pogue, H. Dehghani, C. M. Carpenter, S Jiang, and K. D. Paulsen, "Structural information within regularization matrices improves near infrared diffuse optical tomography," *Opt. Express*, vol. 15, pp. 8043–8058, Jun 2007.

[14] P. K. Yalavarthy, B. W. Pogue, H. Dehghani, and K. D. Paulsen, "Weight-matrix structured regularization provides optimal generalized least-squares estimate in diffuse optical tomography," *Medical Physics*, vol. 34, no. 6, pp. 2085–2098, 2007.

[15] B. Brooksby, S. Jiang, H. Dehghani, B. W. Pogue, K. D. Paulsen, J. Weaver, C. Kogel, and S. P. Poplack, "Combining near-infrared tomography and magnetic resonance imaging to study in vivo breast tissue: implementation of a laplacian-type regularization to incorporate magnetic resonance structure," *Journal of Biomedical Optics*, vol. 10, pp. 051504–051504–10, 2005.

[16] J. A. Fessler and A. O. Hero, "Penalized maximum-likelihood image reconstruction using space-alternating generalized EM algorithms," *IEEE Trans. on Image Proc.*, vol. 4, no. 10, pp. 1417–1429, Oct 1995.

[17] S. J. Wright, R. D. Nowak, and M. A. T. Figueiredo, "Sparse reconstruction by separable approximation," *IEEE Transactions on Signal Processing*, vol. 57, no. 7, pp. 2479–2493, July 2009.

[18] J. Barzilai and J. M. Borwein, "Two-point step size gradient methods," *IMA J. Numer. Anal.*, vol. 8, no. 1, pp. 141–148, 1988.

[19] S. Boyd and L. Vandenberghe, *Convex optimization*, Cambridge University Press, 2004.

[20] A. Beck, "On the convergence of alternating minimization for convex programming with applications to iteratively reweighted least squares and decomposition schemes," *SIAM Journal on Optimization*, vol. 25, no. 1, pp. 185–209, 2015.

[21] Z. T. Harmany, R. F. Marcia, and R. M. Willett, "The Sparse Poisson Intensity Reconstruction ALgorithms (SPIRAL) Toolbox," `http://drz.ac/code/spiraltap/`.

[22] A. H. Barnett, J. P. Culver, A. G. Sorensen, A. Dale, and D. A. Boas, "Robust inference of baseline optical properties of the human head with three-dimensional segmentation from magnetic resonance imaging," *Appl. Opt.*, vol. 42, no. 16, pp. 3095–3108, Jun 2003.

[23] C. Li, G. Wang, J. Qi, and S. R. Cherry, "Three-dimensional fluorescence optical tomography in small animal imaging using simultaneous positron emission tomography priors," *Optics letters*, vol. 34, pp. 2933–2935, 2009.